JOURNAL OF AIRCRAFT
Vol. 35, No. 2, March–April 1998

Experimental Active Control of a Typical Section Using a Trailing-Edge Flap

Jeffrey S. Vipperman,* Robert L. Clark,† Mark Conner,‡ and Earl H. Dowell§
Duke University, Durham, North Carolina 27708-0300

This paper presents an experimental implementation of an active control system used to suppress flutter in a typical section airfoil. The H_2 optimal control system design is based on experimental system identifications of the transfer functions between three measured system variables—pitch, plunge, and flap position—and a single control signal that commands the flap of the airfoil. Closed-loop response of the airfoil demonstrated gust alleviation below the open-loop flutter boundary. In addition, the flutter boundary was extended by 12.4% through the application of active control. Cursory robustness tests demonstrate stable control for variations in flow speed of ±10%.

Introduction

ACTIVE control of articulated aerodynamic control surfaces has been a topic of interest for many years. Various control strategies, including classical, modern linear quadratic regulator/linear quadratic Gaussian (LQG), and robust (H_∞), have been applied to structures ranging in complexity from typical sections[1] to cantilevered wings.[2–4] The objective has typically been twofold: provide gust alleviation for ride quality, and extend the flutter boundary for performance. Although significant effort has been devoted to analytical studies,[5–10] there are fewer experimental implementations of closed-loop controllers.[1–4,11] At the NASA Langley Research Center the Benchmark Active Controls Testbed[12] has been used to generate extensive test data and dynamic models[13] to study flutter-suppression controllers. The physics associated with the control problem are well described.[6,14,15]

The objective of the proposed effort was to investigate experimentally the closed-loop performance of a three-degree-of-freedom (DOF) typical section, using a trailing-edge flap as the control input and measures of pitch, plunge, and flap actuator position as sensor variables. Although analytical models of the system have been developed,[8,16,17] an experimental system identification was performed at each dynamic pressure (flow speed) for which the controller was designed. An H_2 controller was designed that minimized the power associated with pitch, plunge, and flap position upon exciting each state of the measured system with stochastic noise sources. The goal was to create a compensator that would provide gust alleviation at flow speeds well below the flutter boundary and extend the flutter boundary at the upper limit. Based on the experimental system identification, both predicted and measured performance are compared.

Because the poles and zeros of the dynamic system vary as a function of dynamic pressure (flow speed for wind-tunnel experiments), the compensators demonstrated limited robustness to variation in flow speed. In general, the controllers provided stability at flow speeds ±10% of that for which they were designed. Thus, it is not unreasonable to expect a limitation in the extension of the flutter boundary beyond 10%. However, once the flutter boundary is extended, one can identify the system response at the higher flow speed and use this data to design a controller that will stabilize the system at yet higher flow speeds. Because gain scheduling is required, one could identify the closed-loop system on-line and use this data to determine the compensator necessary for operation at higher dynamic pressures.

Received Oct. 26, 1996; revision received July 20, 1997; accepted for publication Aug. 10, 1997.

*Graduate Research Assistant, Department of Mechanical Engineering and Materials Science; currently Assistant Professor of Mechanical Engineering, University of Maine, 5711 Boardman Hall, Orono, ME 04469-5711. Student Member AIAA.

†Assistant Professor, Department of Mechanical Engineering and Materials Science, Box 90300. Member AIAA.

‡Graduate Research Assistant, Department of Mechanical Engineering and Materials Science, Box 90300.

§Dean of Engineering, J. B. Jones Professor of Mechanical Engineering and Materials Science, Box 90300. Fellow AIAA.

Control Strategy

The control system was synthesized by casting the aeroelastic control problem into a two-port configuration using LQG-style weighting parameters (Fig. 1). From Fig. 1, the generalized plant $\boldsymbol{G}(s)$ consists of the aeroelastic model $\{\boldsymbol{A}, \boldsymbol{B}, \boldsymbol{C}, \boldsymbol{D}\}$ as well as subsystems that determine the frequency-domain shape of the process noise, sensor noise, control penalty, and performance penalty, which were chosen to be flat or all-pass. Also from Fig. 1, $\boldsymbol{w}(t)$ is a vector of disturbance inputs composed of process noise $\boldsymbol{\xi}(t)$ and sensor noise $\boldsymbol{\theta}(t)$, which were assumed to be uniform random processes. For simplicity, each state of the aeroelastic model was excited uniformly by $\boldsymbol{\xi}(t)$. The output $\boldsymbol{z}(t)$ is an error or performance vector that allows the performance objective (to minimize pitch, plunge, and flap) to be traded off with control effort. The vector $\boldsymbol{y}(t)$ is the set of measured variables (pitch, plunge, and actuator position) that are fed back to form the scalar control signal $u(t)$ that commands the flap.

Note that the variables measured in $\boldsymbol{y}(t)$ that are fed back to form the control signal are also the plant variables that partially comprise $\boldsymbol{z}(t)$, and are thus minimized by the controller. An experimental system identification is performed to determine $\{\boldsymbol{A}, \boldsymbol{B}, \boldsymbol{C}, \boldsymbol{D}\}$. A total of 27 states were used in the curve-fit, which allowed the less significant dynamics to be modeled as well.

The objective is to find the controller that minimizes the $\|T_{wz}\|_2$ of the closed-loop transfer function from $\boldsymbol{w}$ to $\boldsymbol{z}$: T_{wz} (Doyle et al., 1989), where

$$\|T_{wz}\|_2 := \left\{ \frac{1}{2\pi} \int_{-\infty}^{\infty} \text{trace}[T_{wz}(j\omega)^* T_{wz}(j\omega)]\, d\omega \right\}^{1/2} \tag{1}$$

where $\|\cdot\|_2$ is the 2-norm; T_{wz} is the transfer function from $\boldsymbol{w}$ to $\boldsymbol{z}$ (disturbance input to performance output); * denotes the complex conjugate operator, $j = \sqrt{-1}$; and ω is the natural circular frequency. A block diagram of the quadruple describ-

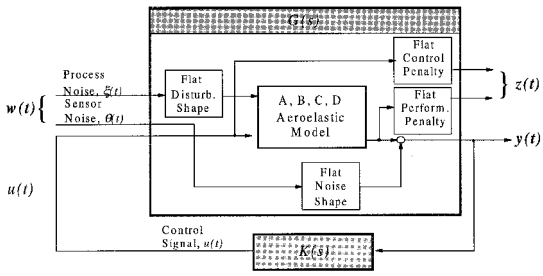

Fig. 1 Diagram of two-port control configuration.

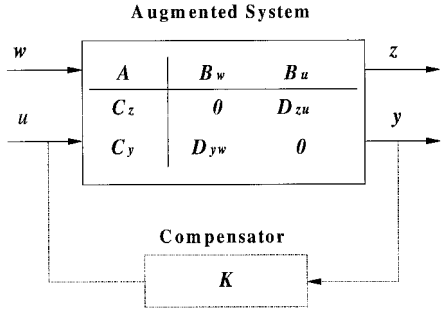

Fig. 2 Composite closed-loop system.

ing the system is illustrated in Fig. 2. The input signals represented by w contain both sensor noise and the disturbance, and z includes both the error signals and the control effort signal. The control input to the moving coil transducer is represented by u, and the measured signals are represented by y. If a frequency-weighted cost functional is desired, one can readily replace the static or all-pass filters included within this model with dynamic filters in formulating the augmented system. Thus, for the chosen formulation, the LQG problem is embedded within the augmented system. The formal solution for the unique optimal controller can be found in Ref. 18.

System Description

Wing Model

The experimental model is shown in Fig. 3. The NACA 0012 rectangular wing model includes two parts: 1) a main wing with a 19-cm chord and 52-cm span, and 2) a flap with a 6.35-cm chord and 52-cm span. The flap is mounted at the trailing edge of the main wing using two pairs of microbearings with pins allowing the flap to have a rotational DOF relative to the main wing. The main wing is constructed from an aluminum alloy circular spar beam with a diameter of 2.54 cm and a wall thickness of 0.32 cm. The beam runs through 14 pieces of NACA 0012 aluminum airfoil plate and serves as the pitch axis, located at the quarter-chord location from the leading edge. A 0.254-mm-thick aluminum sheet covers the entire chord and span, providing the aerodynamic contour of the wing. The flap is constructed in a similar manner, with an aluminum alloy tube spar beam (1.27-cm diameter and 0.16-cm wall thickness) passed through the leading edge of 14 pieces of NACA 0012 wood airfoil plate. The flap is also covered with the same type of aluminum sheet.

The model dimensions were chosen to try to maintain a two-dimensional flowfield by minimizing the end effects and thickness to wall separation. Inertial and stiffness parameters were chosen to yield a flutter speed that was well below the maximum attainable speed for the wind tunnel.

Support Structure

Figure 3 shows the model mounted vertically in the wind tunnel. The support mechanisms for the model are mounted outside of the wind tunnel at the top and bottom. Each support mechanism consists of a guided cantilever beam made of two

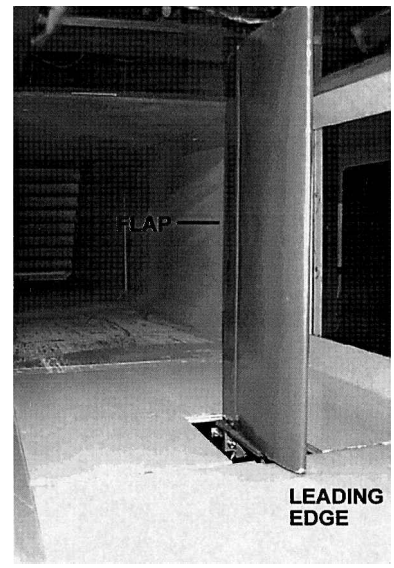

Fig. 3 Experimental model as mounted in the low-speed wind tunnel.

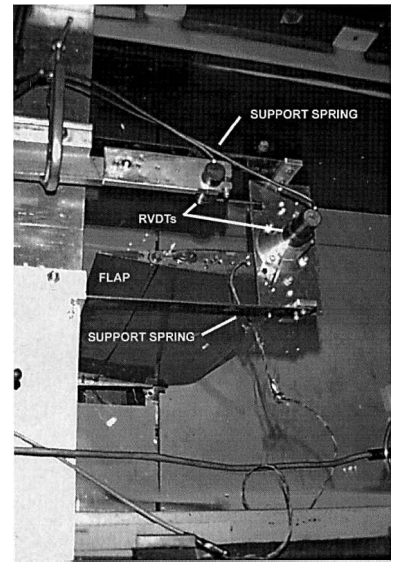

Fig. 4 Top views of the experimental model and the support structure. The airfoil and flap can be seen through the clear top wall of the wind tunnel.

steel leaf springs that are 20.32 cm long, 2.86 cm wide, and 0.102 cm thick.[19] Figure 4 shows the upper support mechanism, which is identical to its lower counterpart. The distance between the two leaf springs that make up each guided cantilever beams is 15.24 cm. A support block joins the free ends of the two leaf springs, and these upper and lower support blocks move with the model along the plunge DOF. The pitch axis of the main wing is mounted to the upper and lower support blocks through a pair of precision bearings that have a small amount of dry friction in the ball. At the upper bracket, a spring wire is press-fit through the center of the shaft that forms the pitch axis and simply supported at each end to form the pitch stiffness. Supports at each end of the spring wire can be moved in or out to increase or decrease, respectively, the stiffness of the pitch axis. The stiffness and inertial properties of the airfoil before the addition of the control actuator assembly can be found in the literature.[16]

Control Actuator Assembly

A schematic of the experimental control assembly is shown in Fig. 5. A linear actuator, LA13-12-000A, serves as the

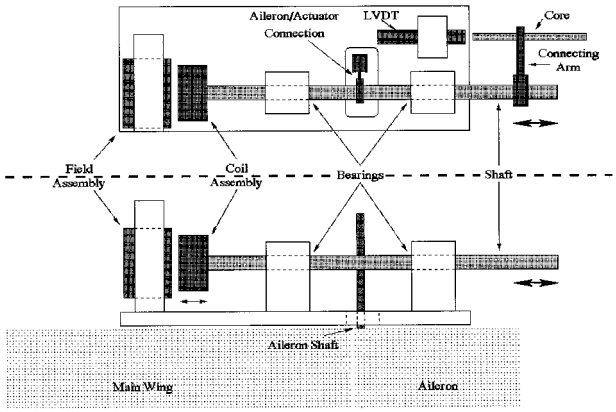

Fig. 5 Schematic diagram of experimental control assembly.

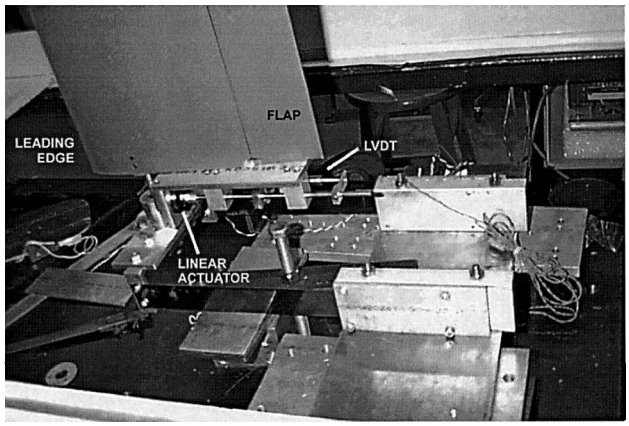

Fig. 6 Control assembly with bottom wall of wind tunnel removed.

means of applying the required control force to the experimental model. The field assembly has a diameter of 3.16 cm, and the coil assembly has a diameter of 2.6 cm. The actuator has a free stroke of ± 0.3175 cm, with a total length (field and coil assemblies) of 2.86 cm at midstroke. The system can apply a peak force of 15.57 N and a blocked force of 7.12 N. The field assembly is held stationary in a support block that is mounted to a base plate used to support all of the control system hardware. Two precision linear bearings are mounted on the base plate and support a mating precision shaft that is threaded into the center of the coil assembly. The bearings allow the coil assembly to move in and out of the field assembly while maintaining the specified clearance between the two. The base plate containing all of the control system hardware is mounted at one end of the wing model, as shown in Fig. 6. The total mass of the actuator assembly is 0.419 kg.

The position of the coil assembly is measured using a Lucas Schaevitz 250-MHR linear variable displacement transducer (LVDT) (Fig. 5). The core of the LVDT is attached to the shaft, and the body of the LVDT is mounted in a support block. In addition to the actuator position, two other displacement measurements are also fed back for the system control. The pitch angle of the main wing is measured by a rotational variable displacement transducer (RVDT), which is fixed at the upper end of the pitch axis. The plunge displacement is measured using another RVDT that remains stationary relative to the motion of the upper support block. Figure 4 indicates the two RVDTs used to measure pitch and plunge. The three measurement signals are independent of each other.

Because the linear motion of the actuator is being converted into the rotational motion of the flap, a small amount of flexibility in the connection is required. The actuator shaft and the shaft extending from the control surface are perpendicular to each other and are joined by a thin, rectangular piece of fairly stiff spring steel, which keeps the actuator shaft from binding as it moves through its entire range of travel. A moment arm that is 2.0 cm long is achieved by the flexible linkage. The entire control assembly is mounted to the lower end of the wing aileron. A cutout must be made in the floor of the tunnel to allow the actuator assembly to extend beyond the main wind-tunnel test section. The cutout is large enough for the control assembly and allows a reasonable range of motion. Because the control system is mounted to the main wing, the entire assembly will pitch and plunge with the airfoil. Flap actuator position was fed back to the control system, in lieu of flap angle, because slightly better coherence with the command signal was measured. The actuator–aileron connector shim added a damped resonance at 125 Hz, which is much higher than the dynamics of the typical section. Measured frequency response functions (FRFs) between flap angle and control input, and flap actuator position and control input, are identical between 0–20 Hz, which encompasses the dynamics of the typical section. Measured airfoil resonances at 6.34, 11.0, and 12.4 Hz (in the absence of flow) are associated with plunge, pitch, and flap DOFs, respectively.

Wind Tunnel

All tests of the two-dimensional wing model were performed in the Duke University low-speed wind tunnel. The wind tunnel is a closed-circuit tunnel with a test section of 0.70×0.51 m and a length of 1.22 m. The maximum attainable airspeed is 89 m/s. The stagnation temperature of the airstream is held constant over a 15–38°C range by means of an external air exchange system and tunnel stagnation pressure equal to the atmospheric pressure at the low-Reynolds number operating conditions. For the present test, the Reynolds number based on model chord is 0.52×10^6.

Controller Implementation

The control designs were implemented in discrete time on a TMS320C31-based digital signal processor (DSP) board manufactured by Spectrum Signal Processing. A Spectrum Signal Processing 16-input, 8-output MIMO board was used to sample the continuous time signals as well as reconstruct digital signals back into analog. Each control design was discretized using a Tustin transform.[20] The controller parameters were downloaded to the DSP using a Pentium®-based computer, which hosted the DSP board.

The sampling rate was set to 2 kHz for all experiments. This provided ample bandwidth for the control problem, which mainly focused on dynamics in a 0–20 Hz frequency band. Most control systems had 25 states after a very modest model reduction, but the final control system, which was based on a system identification performed on a closed-loop system above the original flutter boundary, contained 61 states.

System Identification

To design a controller for experimental implementation, a system identification of the wind-tunnel model was performed. A Tektronix 2630 spectrum analyzer was used to calculate the FRFs and coherences between a random input to the actuator and the resulting responses from each of the three outputs: 1) pitch, 2) plunge, and 3) actuator displacements. The random input signal generated by the Tektronix analyzer was amplified by a Hewlett–Packard 6825A bipolar power supply/amplifier and then sent to the terminals of the linear actuator.

FRF data were recorded for the linear system for freestream conditions ranging from no freestream velocity to speeds near the flutter boundary. SmartID software[21] was then used to perform a multivariable system identification and provide a state–space model of the aeroelastic system. Using 27 states to model the dynamics of the system provided adequate fits for the magnitude and phase for all three transfer functions at each of the flow conditions. The measured magnitude and phase, along with the approximation from the system identification,

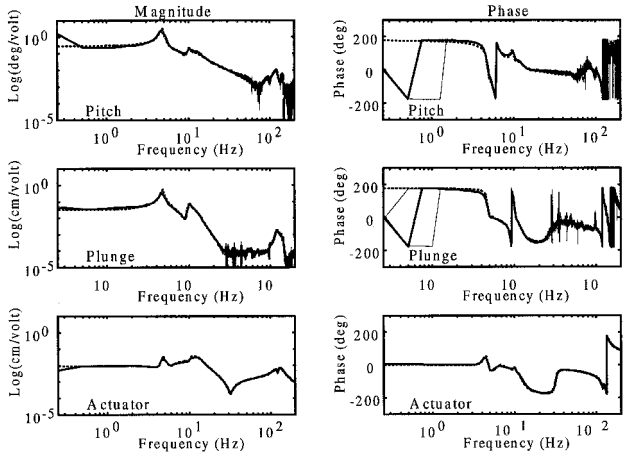

Fig. 7 Measured (——) and modeled (- - -) frequency response of the three observed system variables.

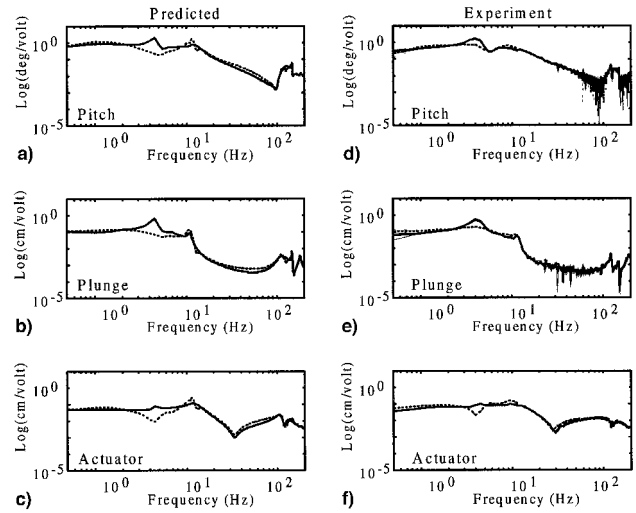

Fig. 8 Analytical and experimental FRFs at a flow of 12.5 m/s: open- (——) and closed-loop (- - -) responses.

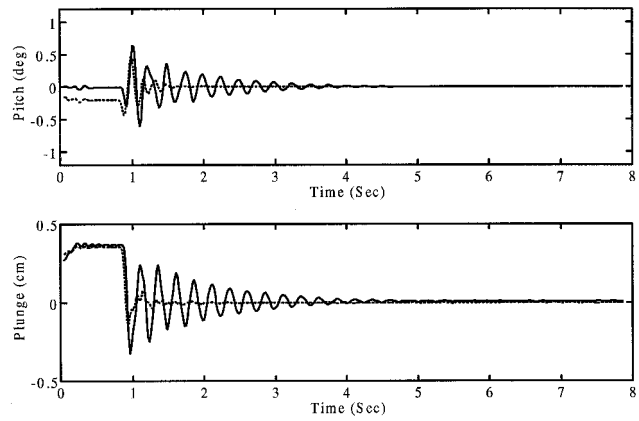

Fig. 9 Transient response with and without control at a flow of 12.5 m/s: open- (——) and closed-loop (- - -) responses.

are shown in Fig. 7 for a representative flow condition of 18.1 m/s. The approximations, which are shown by dotted lines, match well with both the magnitude and phase of the experimentally measured FRFs, which are shown by solid lines. Each frequency-domain experimental FRF has the 95% confidence bounds plotted in very thin lines. It is difficult to see the narrow lines that mark the confidence bounds in Fig. 7 because they are nearly coincident with the bold lines that represent the data. The confidence bounds are computed using an estimate of the coherence function between the input and output signals for the FRF, which takes into account many bias errors, including input noise, estimation biases, nonlinearities, and time-varying properties. The flutter speed for the experimental system without control is approximately 18.6 m/s.

Note that the coherence between the random input to the actuator and the pitch and plunge motion of the typical section model increases as the freestream velocity increases. With the increase in airspeed comes an increase in the fluid–structure coupling that characterizes aeroelastic systems. The increased coupling allows for a more accurate system identification and more controllability, which ameliorates control system design.

Results

Controllers were designed based on each of the system identifications discussed in the preceding text. For the sake of brevity, only two of the preflutter cases will be discussed here. Also, only the magnitude portion of the frequency responses is shown, although the phase data also showed very good correlation.

Low Freestream Velocity

Figures 8a–8c show the predicted open- and closed-loop frequency responses for pitch, plunge, and actuator displacements for a controller designed for an operating flow speed of 12.5 m/s. The predicted responses are obtained by coupling the control designs with the state–space aeroelastic models obtained from the system identification process. The experimental frequency responses are shown in Figs. 8d–8f, including the 95% confidence bounds in very thin lines, which, again, are nearly coincident with the data. The predicted frequencies for the primary and secondary peaks are slightly higher than those of the actual system, though they match well in magnitude. The closed-loop responses are very similar in nature, showing a significant decrease in the magnitude of the primary peak, along with an increase in magnitude at the secondary peak. The numerical model predicted a reduction of approximately 20 dB at the primary peak, but the actual decrease was closer to 15 dB.

The experimental time–domain responses for the pitch and plunge DOFs at 12.5 m/s are shown in Fig. 9. The model was given an initial displacement in the plunge DOF of 3.5 mm and was then released. A significant increase between the overall damping of the open- and closed-loop systems is seen in both of the time series. The controlled system response decays in about one-fourth the time of the uncontrolled system. Confidence bounds for the time–domain plot are not included, because they were characterized in the frequency domain.

High Freestream Velocity

The increased accuracy of the system identification at higher flow conditions can be seen in Fig. 10, which shows the frequency response using a controller designed for an operating freestream velocity of 18.1 m/s. While the correlation between the predicted and experimental frequency responses was very good at the lower flow speed, the predicted and measured open- and closed-loop curves now lie almost on top of each other. The largest difference occurs around 10 Hz, where the numerical model again predicts worse behavior than is seen experimentally. The predicted 20-dB reduction at 4.5 Hz was achieved in the wind-tunnel experiment.

The open-loop or uncontrolled time responses seen in Fig. 11 show that overall system damping is very low and that flow conditions are very near the flutter boundary. The open-loop response continues longer than 7 s, whereas the closed-loop response decays in less than 1.5 s. These results show great potential for increasing the flutter speed.

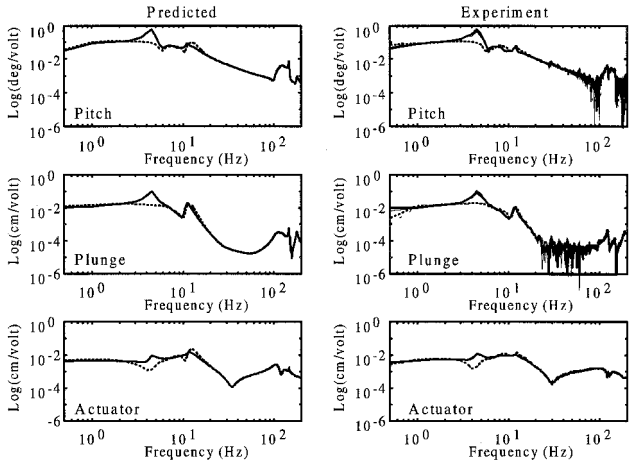

Fig. 10 Open- (——) and closed-loop (---) response at a flow of 18.1 m/s.

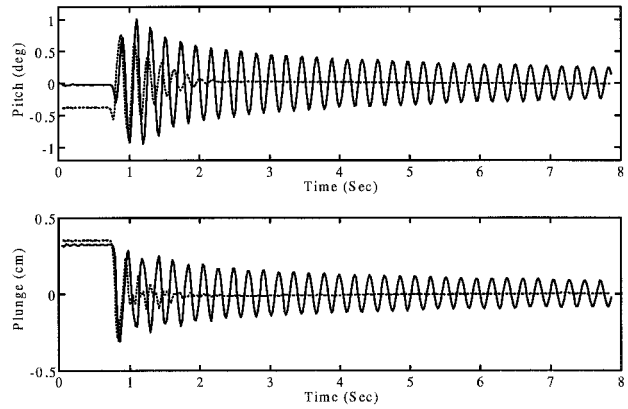

Fig. 11 Transient response with (---) and without (——) control at a flow of 18.1 m/s.

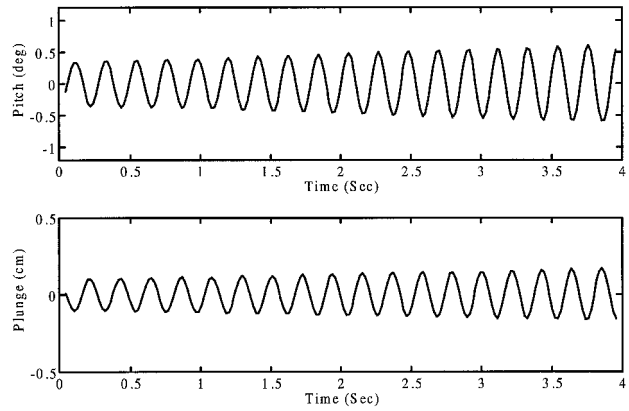

Fig. 12 Unstable transient response without control at a flow of 18.6 m/s.

Flutter Boundary

The flutter speed for the uncontrolled system is approximately 18.6 m/s. Time series for pitch and plunge just past the uncontrolled flutter boundary are shown in Fig. 12. An experimental frequency response was obtained for a freestream velocity of 18.5 m/s, and the controller designed for this flow condition was used to successfully increase the flutter boundary by approximately 8%. Figure 13 shows the controlled time response at 20.0 m/s (8.1% higher than the uncontrolled flutter speed). A closed-loop frequency response was obtained at 20.1 m/s and is shown in Fig. 14a, with the 95% confidence bounds plotted in very thin lines.

Using the postflutter, closed-loop frequency response, a new system identification was performed to obtain a numerical model of the system operating above the uncontrolled flutter boundary. The size of the numerical model increased from 27 states for the preflutter conditions to 50 states at 20.1 m/s. A

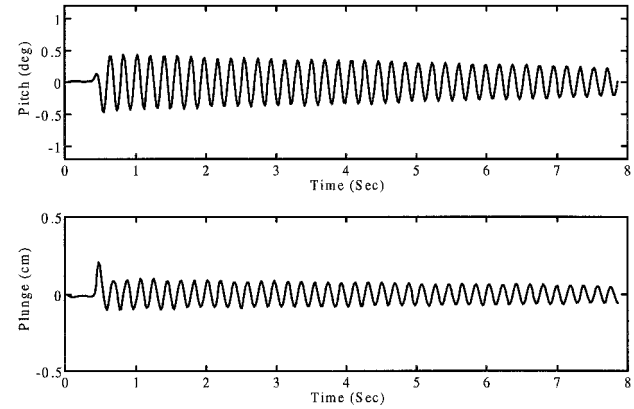

Fig. 13 Closed-loop transient response 8.1% above the uncontrolled flutter boundary.

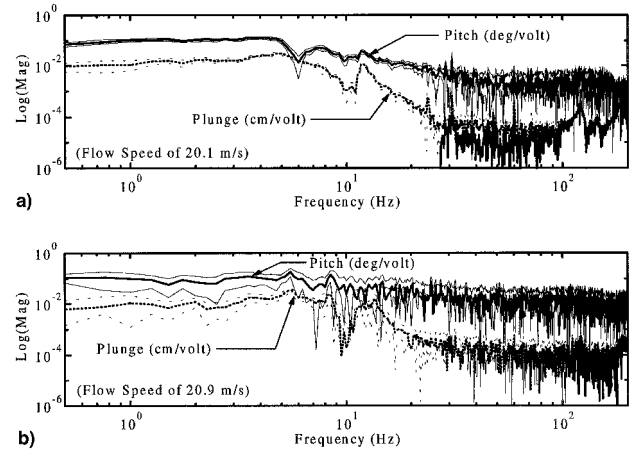

Fig. 14 Closed-loop frequency responses for 20.1 and 20.9 m/s flow rates.

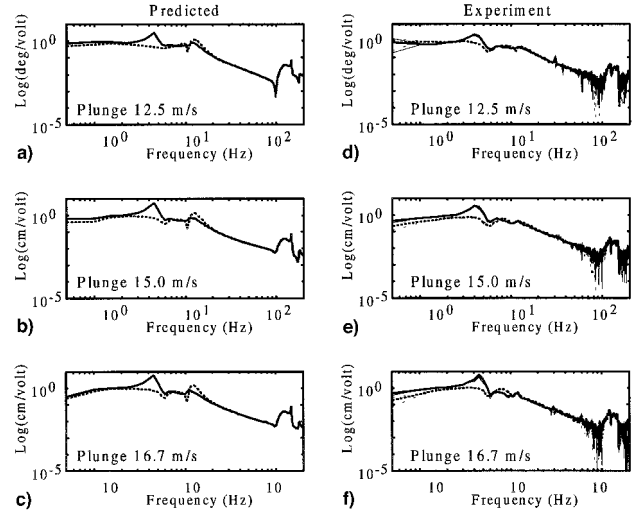

Fig. 15 Open- (——) and closed-loop (---) FRFs for off-nominal flow rates.

new controller was then designed using the new numerical model to try to further increase the flutter boundary. Figure 14b shows the closed-loop frequency response for the experimental system at 20.9 m/s, which represents an overall increase in the original flutter boundary of more than 12%. The 95% confidence bounds plotted in thin lines in Fig. 14b are much larger than those plotted in Fig. 14a because of a decrease in the coherence estimates, presumably caused by the controller interaction and larger aerodynamic excitation at the higher flow rate.

Off-Nominal Design Performance

The effectiveness of each of the controllers away from their nominal design speed was examined numerically and experimentally. Figure 15 shows the open- and closed-loop pitch responses for flow conditions at, above, and below the design speed of 15.0 m/s. The predictions at the lower flow speed of 12.5 m/s show a better correlation with the measured data, as seen in Figs. 15a and 15d. There is a difference in magnitudes at very low frequencies. The same trends are seen between the numerical and experimental data for the higher flow speed of 16.7 m/s, however, there is a noticeable difference in a secondary peak. In this case, the actual response is more favorable than that predicted.

Conclusions

Active control of a typical section airfoil using a trailing-edge flap as the control input and measures of pitch, plunge, and flap actuator position as sensor variables was investigated. An experimental system identification was performed at each dynamic pressure (flow speed for wind-tunnel experiments), and an H_2 controller was designed for each flow condition to minimize the root-mean-square power associated with the pitch, plunge, and flap position caused by stochastic disturbance sources applied across each aeroelastic state of the system. The resulting compensator provided gust alleviation at flow speeds well below the flutter boundary and extended the flutter boundary at the upper limit by 12.4%. The predicted and measured closed-loop performance compared well over all flow conditions, and the resulting compensators designed for a specific flow condition were observed to provide stable closed-loop performance at flow speeds varying $\pm 10\%$ of the nominal.

Results from this work also demonstrate that once the flutter boundary is extended through the implementation of an active control system, a system identification of the closed-loop system can be obtained to design a controller that further extends the flutter boundary for higher flow speeds. If the controller were designed on-line, then one could identify the plant concurrently while implementing control to meet the demands of variation in dynamic pressure.

Future work will address the effects of free-play nonlinearities between the flap actuator and the flap. In addition, methods of producing a robust control system for all operating conditions (dynamic pressures) using gain-scheduling or structured uncertainty methods will be investigated.

Acknowledgments

The authors gratefully acknowledge the U.S. Air Force Office of Scientific Research for funding this research under Grant F49620-92-J-0491, monitored by Brian Sanders. The authors also are grateful to David Cox of the Guidance Controls Branch at NASA Langley Research Center for his helpful insight into the control system design. Special thanks are extended to the anonymous reviewer whose thorough review and comments helped improve the quality of this paper.

References

[1]Mukhopadhyay, V., "Flutter Suppression Control Law Design and Testing for the Active Flexible Wing," *Journal of Aircraft*, Vol. 32, No. 1, 1995, pp. 45–51.

[2]Lin, C. Y., Crawley, E. F., and Heeg, J., "Open Loop and Preliminary Closed Loop Results of a Strain Actuated Active Aeroelastic Wing," *AIAA/ASME/ASCE/AHS/ASC 36th Structures, Structural Dynamics, and Materials Conference* (New Orleans, LA), AIAA, Washington, DC, 1995, pp. 1904–1914.

[3]Ghiringhelli, G. L., Lanz, M., and Mantegazza, P., "Active Flutter Suppression for a Wing Model," *Journal of Aircraft*, Vol. 27, No. 4, 1990, pp. 334–341.

[4]Pak, C., Friedmann, P. P., and Livne, E., "Transonic Adaptive Flutter Suppression Using Approximate Unsteady Time Domain Aerodynamics," *AIAA/ASME/ASCE/AHS/ASC 32nd Structures, Structural Dynamics, and Materials Conference*, AIAA, Washington, DC, 1991, pp. 1832–1854.

[5]Ozbay, H., and Bachmann, G. R., "H_2/H_∞ Controller Design for a Two-Dimensional Thin Airfoil Flutter Suppression," *Journal of Guidance, Control, and Dynamics*, Vol. 17, No. 4, 1994, pp. 722–728.

[6]Edwards, J. W., Breakwell, J. V., and Bryson, A. E., "Active Flutter Control Using Generalized Unsteady Aerodynamic Theory," *Journal of Guidance and Control*, Vol. 1, No. 1, 1978, pp. 32–40.

[7]Lazarus, K. B., Crawley, E. F., and Lin, C. Y., "Fundamental Mechanisms of Aeroelastic Control with Control Surface and Strain Actuation," *Journal of Guidance, Control, and Dynamics*, Vol. 18, No. 1, 1995, pp. 10–17.

[8]Conner, M. D., Tang, D., Dowell, E. H., and Virgin, L. N., "Accurate Numerical Integration of State-Space Models for Aeroelastic Systems with Freeplay," *AIAA Journal*, Vol. 34, 1996, pp. 2202–2205.

[9]Newsom, J. R., "Control Law Synthesis for Active Flutter Suppression Using Optimal Control Theory," *Journal of Guidance and Control*, Vol. 2, No. 5, 1979, pp. 388–394.

[10]Lin, C. Y., and Crawley, E. F., "Design Considerations for a Strain Actuated Adaptive Wing for Aeroelastic Control," *Proceedings of the 4th International Conference on Adaptive Structures* (Cologne, Germany), 1993.

[11]Lazarus, K. B., Crawley, E. F., and Lin, C. Y., "Multivariable Active Lifting Surface Control Using Strain Actuation: Analytical and Experimental Results," *Journal of Aircraft*, Vol. 34, No. 3, 1997, pp. 313–321.

[12]Durham, M. H., Keller, D. F., Bennett, R. M., and Wieseman, C. D., "A Status Report on a Model for Benchmark Active Controls Testing," AIAA Paper 91-1011, 1991.

[13]Waszak, M. R., "Modeling the Benchmark Active Control Technology Wind-Tunnel Model for Application to Flutter Suppression," *Proceedings of the AIAA Atmospheric Flight Mechanics Conference* (San Diego, CA), 1996.

[14]Karpel, M., "Design for Active Flutter Suppression and Gust Alleviation Using State-Space Aeroelastic Modeling," *Journal of Aircraft*, Vol. 19, No. 3, 1982, pp. 221–227.

[15]Lazarus, K. B., and Crawley, E. F., "Multivariable High-Authority Control of Plate-Like Active Structures," *AIAA/ASME/ASCE/AHS/ASC 33rd Structures, Structural Dynamics, and Materials Conference* (Dallas, TX), AIAA, Washington, DC, 1992, pp. 931–945.

[16]Conner, M. D., Tang, D., Dowell, E. H., and Virgin, L. N., "Nonlinear Behavior of a Typical Airfoil Section with Control Surface Freeplay: A Numerical and Experimental Study," *Journal of Fluids and Structures*, Vol. 11, No. 1, 1997, pp. 89–109.

[17]Conner, M. D., "Nonlinear Aeroelasticity of an Airfoil Section With Control Surface Freeplay," Ph.D. Dissertation, Duke Univ., Durham, NC, 1996.

[18]Doyle, J. C., Glover, K., Khargonekar, P. P., and Francis, B. A., "State-Space Solutions to Standard H_2/H_∞ Control Problems," *IEEE Transactions on Automatic Control*, Vol. 34, No. 8, 1989, pp. 831–847.

[19]Roark, R. J., and Young, W. C., *Roark's Formulas for Stress and Strain*, McGraw–Hill, New York, 1989.

[20]Oppenheim, A. V., and Schafer, R. W., *Digital Signal Processing*, Prentice–Hall, Englewood Cliffs, NJ, 1975.

[21]Smart ID System Identification Software, Active Control eXperts, Cambridge, MA.